Peptides of Matrix Gla Protein Inhibit Nucleation and Growth of Hydroxyapatite and Calcium Oxalate Monohydrate Crystals

Maria Goiko[1], Joshua Dierolf[2], Jared S. Gleberzon[3], Yinyin Liao[2], Bernd Grohe[2], Harvey A. Goldberg[2,3], John R. de Bruyn[1], Graeme K. Hunter[2,3]*

1 Department of Physics & Astronomy, University of Western Ontario, London, Canada, **2** School of Dentistry, University of Western Ontario, London, Canada, **3** Department of Biochemistry, University of Western Ontario, London, Canada

Abstract

Matrix Gla protein (MGP) is a phosphorylated and γ-carboxylated protein that has been shown to prevent the deposition of hydroxyapatite crystals in the walls of blood vessels. MGP is also expressed in kidney and may inhibit the formation of kidney stones, which mainly consist of another crystalline phase, calcium oxalate monohydrate. To determine the mechanism by which MGP prevents soft-tissue calcification, we have synthesized peptides corresponding to the phosphorylated and γ-carboxylated sequences of human MGP in both post-translationally modified and non-modified forms. The effects of these peptides on hydroxyapatite formation and calcium oxalate crystallization were quantified using dynamic light scattering and scanning electron microscopy, respectively. Peptides YGlapS (MGP1-14: YγEpSHEpSMEpSYELNP), YEpS (YEpSHEpSMEpSYELNP), YGlaS (YγESHESMESYELNP) and SK-Gla (MGP43-56: SKPVHγELNRγEACDD) inhibited formation of hydroxyapatite in order of potency YGlapS > YEpS > YGlaS > SK-Gla. The effects of YGlapS, YEpS and YGlaS on hydroxyapatite formation were on both crystal nucleation and growth; the effect of SK-Gla was on nucleation. YGlapS and YEpS significantly inhibited the growth of calcium oxalate monohydrate crystals, while simultaneously promoting the formation of calcium oxalate dihydrate. The effects of these phosphopeptides on calcium oxalate monohydrate formation were on growth of crystals rather than nucleation. We have shown that the use of dynamic light scattering allows inhibitors of hydroxyapatite nucleation and growth to be distinguished. We have also demonstrated for the first time that MGP peptides inhibit the formation of calcium oxalate monohydrate. Based on the latter finding, we propose that MGP function not only to prevent blood-vessel calcification but also to inhibit stone formation in kidney.

Competing interests: The authors have declared that no competing interests exist.

* E-mail: graeme.hunter@schulich.uwo.ca

Introduction

Matrix gla protein (MGP) is a phosphorylated and γ-carboxylated protein expressed at high levels in heart, lung and kidney [1]. MGP is a highly conserved 84-amino acid protein that contains 5 residues of γ-carboxyglutamic acid (gla): one at amino acid 2 and the rest in the centre of the molecule (amino acids 37, 41, 48 and 52) [2]. In addition, there are 3 sites of serine phosphorylation near the N-terminus (amino acids 3, 6 and 9) [3]. The C-terminal third of MGP is quite hydrophobic, and consequently the protein is poorly soluble [2,4,5]. Apparently for this reason, very little is known about MGP's structure, although one study reported that synthetic MGP (γ-carboxylated but not phosphorylated) has ~21% α-helix [5].

Mice lacking the *Mgp* gene exhibit massive calcification of the medial layer of blood vessels and die from arterial rupture soon after birth [6]. A similar pattern of calcification is seen when rats are given the vitamin K antagonist warfarin, which inhibits γ-carboxylation, implicating the gla residues of MGP in the anticalcification function of the protein [7]. In humans, expression of the *Mgp* gene is upregulated in human atherosclerotic plaque [8], suggesting that the protein is an inducible inhibitor of calcification. Although undercarboxylation of MGP is associated with aortic stenosis [9], warfarin treatment does not cause a significant increase in coronary artery calcification [10]. Nonetheless, it appears clear that MGP functions as an inhibitor of blood-vessel calcification, and that the gla residues play an important role in this process.

To further investigate the role of post-translational modifications in the anti-calcification activity of MGP, Schurgers et al. studied cultures of vascular smooth muscle cells. In media containing high concentrations of calcium and/or phosphate, these cultures produce a calcified matrix; like atherosclerotic plaque, the mineral phase is hydroxyapatite (HA). Addition of synthetic peptides corresponding to full-length MGP, amino acids 35-54 or amino acids 3-15 inhibited calcification of vascular smooth muscle cells at a concentration of 200 nM, while non-post-translationally modified versions of these molecules had no significant effects [11].

The above-mentioned studies did not address the mechanism by which MGP inhibits calcification. We hypothesized that MGP adsorbs to HA and inhibits further growth of the crystals, which has previously been shown for other calcification-inhibiting proteins [12]. To test this hypothesis, we used a combination of simulation and experimentation. For simulation of the adsorption of MGP to HA, the 84-residue human MGP sequence was divided into six 14-amino-acid virtual peptides: YGlapS, FIN, QR-Gla, SK-Gla, YRL and AAY. The interaction of each sequence with the {100} and {001} faces of HA studied by molecular dynamics. Peptide YGlapS contains one gla and 3 phosphoserines, and was therefore also simulated in non-γ-carboxylated (YEpS), non-phosphorylated (YGlaS) and non-γ-carboxylated/non-phosphorylated (YES) forms. QR-Gla and SK-Gla each contain two glas, and therefore were also synthesized in non-γ-carboxylated forms (QR-E and SK-E, respectively). In the experimental arm of the study, synthetic peptides corresponding to each of the virtual peptides were synthesized. Inhibition of HA growth by the synthetic MGP peptides was quantified by the constant-composition/seeded growth method [13]. Results from simulation and experimentation were in excellent agreement. Peptides YGlapS (YγEpSHEpSMEpSYELNP) and SK-Gla (SKPVHγELNRγEACDD) adsorbed most strongly to HA and were also potent inhibitors of HA growth (IC$_{50}$ values of 1.48 and 2.92 μM, respectively). The adsorption and inhibitory activities of YGlapS were dependent upon phosphorylation but not γ-carboxylation, whereas those of SK-Gla were dependent upon γ-carboxylation [14]. These findings suggest that MGP inhibits arterial calcification by adsorbing to and inhibiting the growth of HA crystals, and that this activity involves the phosphorylated N-terminus and central gla-containing region of the protein.

MGP is expressed at high levels in kidney [1,15,16] and its expression is upregulated in animal models of kidney-stone disease [17,18]. In addition, a polymorphism of the *Mgp* gene has been linked to stone disease in Japanese [19] and Chinese [20] populations. This raises the possibility that MGP plays a role in preventing the ectopic calcification of kidney. Unlike atherosclerotic plaque, kidney stones contain a variety of mineral phases. While calcium oxalates (CaOx) are the most abundant, HA and other calcium phosphates are also often present in stones [21,22].

Crystal formation involves two processes: nucleation and growth. In the present study, we have examined the effects of synthetic MGP peptides on the *in vitro* formation of HA by dynamic light scattering (DLS), which, unlike the constant-composition/seeded growth method used in our previous study [14], allowed us to examine the effects of these peptides on crystal nucleation. Because CaOx crystals tend to nucleate on surfaces rather than in solution, DLS cannot be used. Instead, we employed scanning electron microscopy to study the effects of MGP peptides on the nucleation and growth of calcium oxalate monohydrate (COM) and calcium oxalate dihydrate (COD) crystals. The non-post-translationally modified MGP peptides FIN (MGP15-28), AAY (MGP57-70), and YRL (MGP71-84) were not included in the present analysis because they exhibited no adsorption to HA or inhibition of HA growth in our previous study [14]. QR-Gla (MGP29-42) and QR-E (non-γ-carboxylated MGP29-42) were studied, but had no significant effects on HA or CaOx formation. Therefore, data from these peptides are not included here.

Methods

Physicochemical characterization of peptides

MGP peptides were synthesized as previously described [14]. The physicochemical characteristics of these peptides are listed in Table 1. Isoelectric points (pI), net charges and hydrophilicity values were determined as previously described [23]. Hydrophilicity data were calculated on the basis of an empirical hydrophilicity scale for individual amino acids elaborated by Hopp and Woods [24]. Estimation of hydrophilicity data for posttranslational modifications (e.g. phosphate, γ-carboxyglutamate) were carried out as previous described [23].

Circular dichroism spectropolarimetry

Circular dichroism spectra were recorded using a Jasco J-810 spectropolarimeter connected to a Peltier temperature-control system. Peptides were dissolved at a concentration of 0.22 mg/mL in distilled water. Scans were measured from 200 nm to 260 nm. Each peptide solution was scanned at 37°C in a cell with a path length of 1 mm, with a scan speed of 100 nm/min and step size of 0.5 nm. Solutions were scanned 10 times and the resulting spectra were averaged. After subtraction of blank (water) scans, peptide raw data were converted to mean residue ellipticity (θ) in units of degree cm^2 dmol^{-1} by standard procedures. CONTINLL, CDSSTR and SELCON3 algorithms were used to estimate peptide secondary structure from the UV CD spectra generated with the protein reference set "SMP50." Estimates from the three algorithms were then averaged using Prism 4 (GraphPad).

Hydroxyapatite growth

Three working solutions were prepared daily as described in [25], composed of 24 mM CaCl$_2$, 150 mM NaCl and 18.75 mM Tris (calcium solution); 15 mM Na$_2$HPO$_4$, 150 mM NaCl and 18.75 mM Tris (phosphate solution); and 150 mM NaCl and 18.75 mM Tris (Tris solution). For each experimental run, measured volumes of the calcium and phosphate solutions were added to Tris solution containing the desired concentration of peptide (0-10 μg/ml) in a 5-ml borosilicate

Table 1. Chemical characteristics of MGP peptides.

Peptide	Sequence	M_W [A] [g/mol]	Isoelectric point [B]	Net charge at pH 6.7 / 7.4 [B]	Hydrophilicity [kJ/mol] [C]
YGlapS	YγEpSHEpSMEpSYELNP	1998.8	2.23	- 8.6/- 9.1	56.5/4.03
YEpS	YEpSHEpSMEpSYELNP	1954.7	2.36	- 8.1/- 8.6	54.4/3.89
YGlaS	YγESHESMESYELNP	1758.7	3.84	- 4.1/- 4.6	22.6/1.61
YES	YESHESMESYELNP	1714.8	4.00	- 3.6/- 4.1	20.5/1.46
SK-Gla	SKPVHγELNRγEACDD	1700.8	4.52	- 2.7/- 3.2	59.4/4.24
SK-E	SKPVHELNRγEACDD	1612.8	4.89	- 1.7/- 2.2	55.2/3.94

[A] Molecular weight (electrospray mass spectrometry); [B] (http://ca.expasy.org, different tools); [C] Data are given for the complete molecule and the amino acid average within that molecule, calculated on basis of the empirical hydrophilicity scale of Hopp and Woods [24] and by estimation of hydrophilicity data for posttranslational modifications [23].

doi: 10.1371/journal.pone.0080344.t001

glass tube, giving a final volume of 1.8 ml. The ratio of Ca^{2+} and PO_4^{3-} concentrations in the resultant solution was fixed at 1.60. The concentrations of Ca^{2+} and PO_4^{3-} were chosen to give a reasonable rate of crystal formation (intensity of ~100 kHz by the end of the experiment) in control runs with no added peptide. The level of supersaturation required for this varied from day to day, presumably because of minor variations in temperature, pH and presence of impurities. For YGlapS, YEpS, YGlaS and YES, [Ca] = 5.67 mM and [PO_4] = 3.54 mM; for SK-Gla, [Ca] = 7.33 mM and [PO_4] = 4.58 mM; for SK-E, [Ca] = 7.00 mM and [PO_4] = 4.38 mM. All measurements for a given peptide were performed within a span of six to eight hours. The effects of various peptide concentrations on HA formation were compared to that day's control. Solutions were prepared and experiments performed at room temperature.

Dynamic light scattering

Dynamic light scattering experiments were performed using an ALV CGS-3 goniometer-based light scattering system. The procedure and data analysis were similar to those described in ref [25].. Scattering data were collected over a period of forty minutes immediately following the preparation of a crystal-forming solution. The autocorrelation function of the scattered light intensity and the mean scattered intensity I_m were automatically calculated and saved at 30-s intervals. I_m increases with both the concentration and size of the scattering particles. The electric field autocorrelation function was calculated from the measured intensity autocorrelation function using the Siegert relation [26]. The mean hydrodynamic ($\overline{r_h}$) of the scattering particles at each 30-s time step was determined from the decay of field autocorrelation function using the method of cumulants [27] and a standard nonlinear least-squares fitting algorithm.

Calcium oxalate growth

To study effects of MGP peptides on COM and COD growth habit and volumes of precipitate, crystals were grown on freshly cleaved mica from solutions containing [Ca^{2+}] = [$C_2O_4^{2-}$] = 1 mM as previously described [28,29]. Under these conditions, the supersaturation (calculated as σ = 1/2 ln [$a_{Ca} \cdot a_{Ox}/K_{SP}$] [23]) was 2.86 for COM and 2.31 for COD using solubility products K_{SP} for COM ($K_{SP;COM}$ = 2.24 · 10^{-9} M^2) or

COD ($K_{SP;COD}$ = 6.76 · 10^{-9} M^2) at 37°C [30]. Peptides were studied at 0-20 µg/ml.

Scanning electron microscopy

Scanning electron microscopy (SEM; A LEO 1540XB, Carl Zeiss, Germany) was used to study the precipitates on mica substrates without metal coating, at an acceleration voltage of 1 kV and a working distance of 3.5-4.0 mm. Using SEM micrographs, COM <001> and <010> dimensions were measured from six {100}-nucleated crystals, and <001> and <100> dimensions were measured from six {010}-nucleated crystals. Volumes were calculated as mean area of the {100} face x mean <010> dimension x number of crystals/mm^2 [23,29]. COD dimensions were analyzed from six crystals nucleated from various orientations. Data from each crystal (e.g., edge length, angles) were entered in a calculation routine and crystal volumes determined. Overall volumes were calculated as mean crystal volume x number of crystals/mm^2, as previous described [23,29]. Data were analyzed by one-way analysis of variance followed by Dunnett's multiple correlations test using Prism 4 (GraphPad).

Results

Structure of MGP peptides

The sequences and physicochemical properties of the MGP peptides used in this study are shown in Table 1. The secondary structures of these peptides were studied by circular dichroism spectropolarimetry (Figure 1). Deconvolution of the CD spectra indicated that these peptides are approximately 35% unordered with low helical content and high contents of turn and β-strand (Table 2).

Effects of MGP peptides on HA nucleation and growth

The effects of MGP peptides on HA formation were studied by dynamic light scattering (DLS). Figure 2 shows plots of DLS intensity against time for peptide YGlapS and its variants, YGlaS, YEpS and YES, as well as SK-Gla and its variant, SK-E. DLS intensity is a function of both the size and number of scattering particles. Of the 6 peptides studied, YGlapS resulted in the greatest decreases in intensity, with the maximal effect occurring at 3 µg/ml (Figure 2A). YEpS, the non-γ-carboxylated
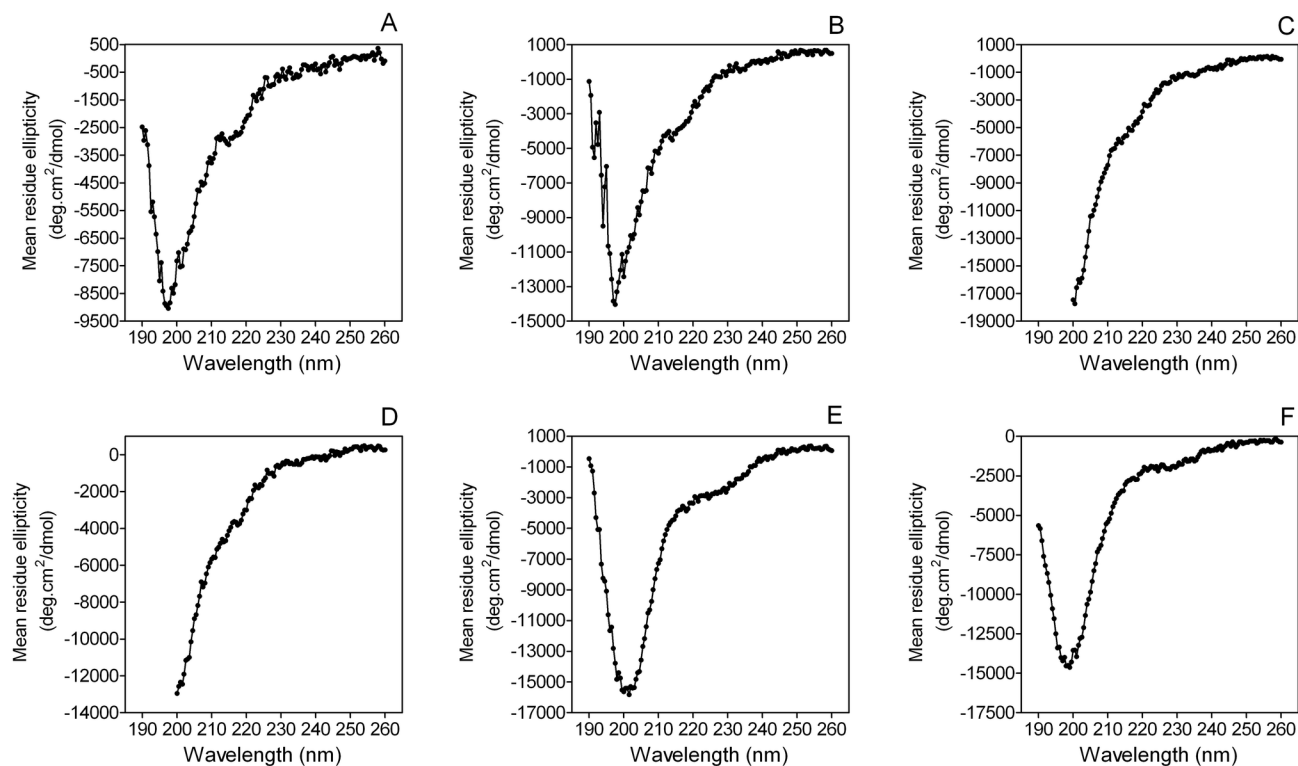
Figure 1. Circular dichroism spectropolarimetry analyses of MGP peptides. A. YGlapS B. YEpS C. YGlaS D. YES E. SK-Gla F. SK-E .

doi: 10.1371/journal.pone.0080344.g001

Table 2. Analysis of circular dichroism spectropolarimetry of MGP peptides.

Peptide	α-helix	Distorted α-helix	β-strand	Distorted β-strand	Turn	Unordered
YGlapS	0.9±0.8	5.6±1.8	23.9±0.9	13.1±0.6	20.6±1.9	30.5±4.1
YEpS	0.1±0.1	3.7±1.43	22.2±1.43	14.1±0.2	22.4±0.2	36.8±0.8
YGlaS	0.3±0.3	5.4±1.2	19.1±1.1	13.2±0.3	25.3±0.5	35.7±1.42
YES	1.1±1.0	2.2±2.1	12.8±7.8	10.8±2.1	29.2±5.7	44.1±5.7
SK-Gla	2.1±1.7	8.1±1.9	19.1±2.3	11.6±0.2	23.8±1.9	33.4±3.7
SK-E	1.9±1.2	5.7±1.6	19.1±2.0	11.8±0.1	23.4±0.3	38.7±1.2

Spectra shown in Figure 1 were analyzed with CDPro. Secondary structures percentages derived by the CONTINLL, CDSSTR and SELCON3 algorithms were averaged (± SEM).

doi: 10.1371/journal.pone.0080344.t002

version of this peptide, was almost as potent (Figure 2B). YGlapS, the nonphosphorylated version of YGlapS, was less potent than YEpS, with 7 µg/ml peptide required to maximally decrease the change in intensity with time (Figure 2C). YES, which is neither γ-carboxylated nor phosphorylated, resulted in only a small decrease in intensity at 10 µg/ml, whereas lower concentrations appeared to promote crystallization (Figure 2D). These findings indicate that both the 3 phosphate groups and the single γ-carboxylate group contribute to the HA-inhibiting effect of YGlapS.

Increasing concentrations of SK-Gla caused decreased DLS intensities (Figure 2E), although the effect was less than that of

YGlapS or YEpS (Figure 2A, B), with some crystal formation occurring at 10 µg/ml. SK-E had no significant effect on intensity (Figure 2F), showing that the inhibitory effect of SK-Gla is critically dependent upon γ-carboxylation of this peptide.

To compare the effects of YGlapS, YEpS and YGlaS on HA formation, intensities at the end of the incubation were plotted against peptide concentration (Figure 3A). From these plots, peptide concentrations causing half-maximal effect on intensity ($IC_{50}I$) could be calculated. The $IC_{50}I$ values for YGlapS, YEpS and YGlaS were 0.467 µg/ml (0.234 µM), 0.654 µg/ml (0.335 µM) and 4.92 µg/ml (2.80 µM), respectively.

E. SK-Gla .
F. SK-E .
Red – control, blue - 1 µg/ml, green - 3 µg/ml, magenta - 5 µg/ml, grey - 7 µg/ml, orange - 10 µg/ml.
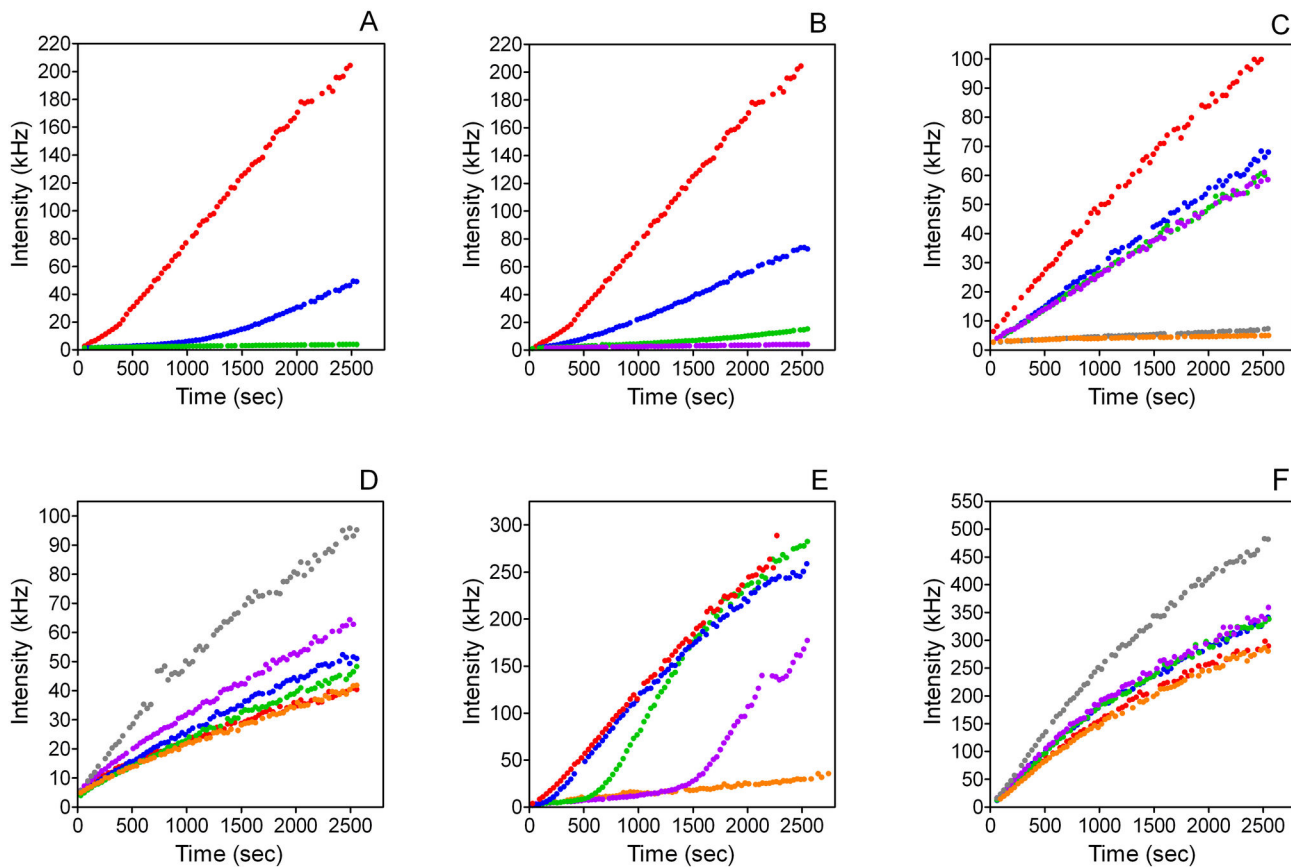
Figure 2. Effects of MGP peptides on intensity of dynamic light scattering. A. YGlapS .
B. YEpS .
C. YGlaS .
doi: 10.1371/journal.pone.0080344.g002
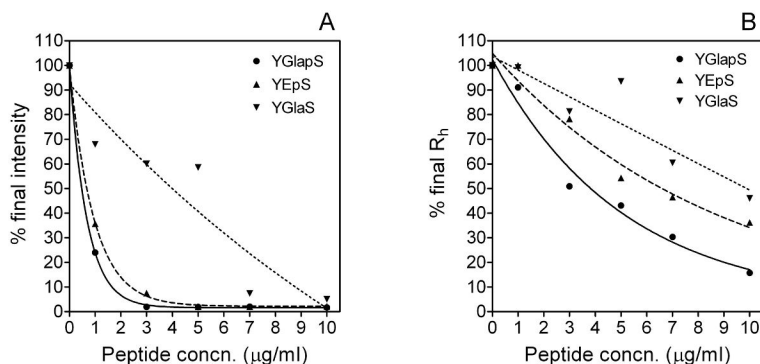
Figure 3. Effects of YGlapS and YEpS on HA formation as measured by dynamic light scattering. A. Intensity.
B. Hydrodynamic radius.
Data from Figures 2 and 4 were used. For YGlapS and YEpS, data were fitted to one-site exponential decay curves. Data for YGlaS were analyzed by linear regression.
doi: 10.1371/journal.pone.0080344.g003

E. SK-Gla.

F. SK-E .

Red – control, blue - 1 μg/ml, green - 3 μg/ml, magenta - 5 μg/ml, grey - 7 μg/ml, orange - 10 μg/ml.
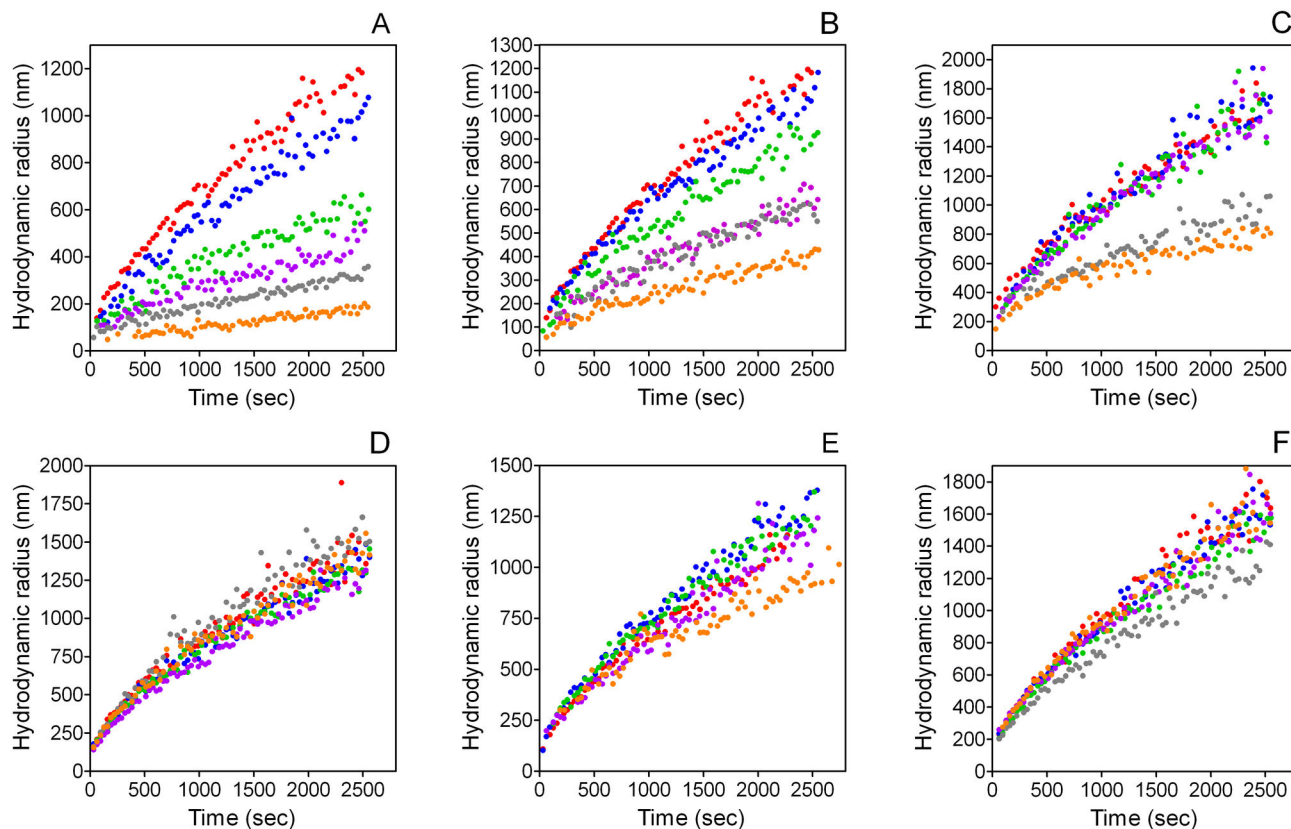
Figure 4. Effect of MGP peptides on hydrodynamic radii (R_h) as measured by dynamic light scattering. A. YGlapS.
B. YEpS.
C. YGlaS.

doi: 10.1371/journal.pone.0080344.g004

Hydrodynamic radius (R_h) measurements are shown in Figure 4. YGlapS decreased R_h in a concentration-dependent manner (Figure 4A). YEpS and YGlaS also caused decreases in R_h, although the effects are less dramatic than that of YGlapS (Figure 4B, C). YES and SK-E did not have significant effects on R_h (Figure 4D, F). SK-Gla slightly decreased R_h (Figure 4E).

To compare the effects of YGlapS, YEpS and YGlaS on HA growth, final R_h values were plotted against peptide concentration (Figure 3B). The calculated $IC_{50}R_h$ values for YGlapS, YEpS and YGlaS were 3.53 μg/ml (1.76 μM), 6.15 μg/ml (3.15 μM), and 9.56 μg/ml (5.44 μM), respectively.

Whereas R_h is a well-defined measure of characteristic crystal size, intensity is a complex function of both crystal size and concentration. To determine the effects of MGP peptides on the concentration of crystals, and therefore on nucleation of HA, we plotted intensities against corresponding R_h values for all concentrations of each peptide (Figure 5). If a peptide causes a decrease in intensity at a given R_h value, this can only be due to a decreased concentration of crystals (implying

inhibition of nucleation). The log-log plots shown in Figure 5 exhibit a sigmoid relationship between intensity and R_h for control (peptide-free) solutions. Addition of YGlapS results in less-steep gradients at all concentrations ≥3 μg/ml, showing that these concentrations inhibit HA nucleation (Figure 5A). For YEpS, concentrations ≥5 μg/ml inhibited nucleation, as shown by decreased gradients compared to control (Figure 5B). For YGlapS, inhibition of HA nucleation was only observed at peptide concentrations ≥7 μg/ml (Figure 5C). The remaining peptides – YES, SK-Gla and SK-E – had no effect on nucleation (Figure 5D, E, F). This analysis suggests that YGlapS is a more potent inhibitor of HA nucleation than YEpS, which in turn is more potent than YGlaS.

Effects of MGP peptides on calcium oxalate crystallization

As calcium oxalate crystals prefer to nucleate on charged surfaces rather than in solution, we were unable to use DLS for these studies. Instead, we used SEM to quantify COM and COD formed in the presence of MGP peptides at

E. SK-Gla.
F. SK-E.
Red – control, blue - 1 µg/ml, green - 3 µg/ml, magenta - 5 µg/ml, grey - 7 µg/ml, orange - 10 µg/ml.
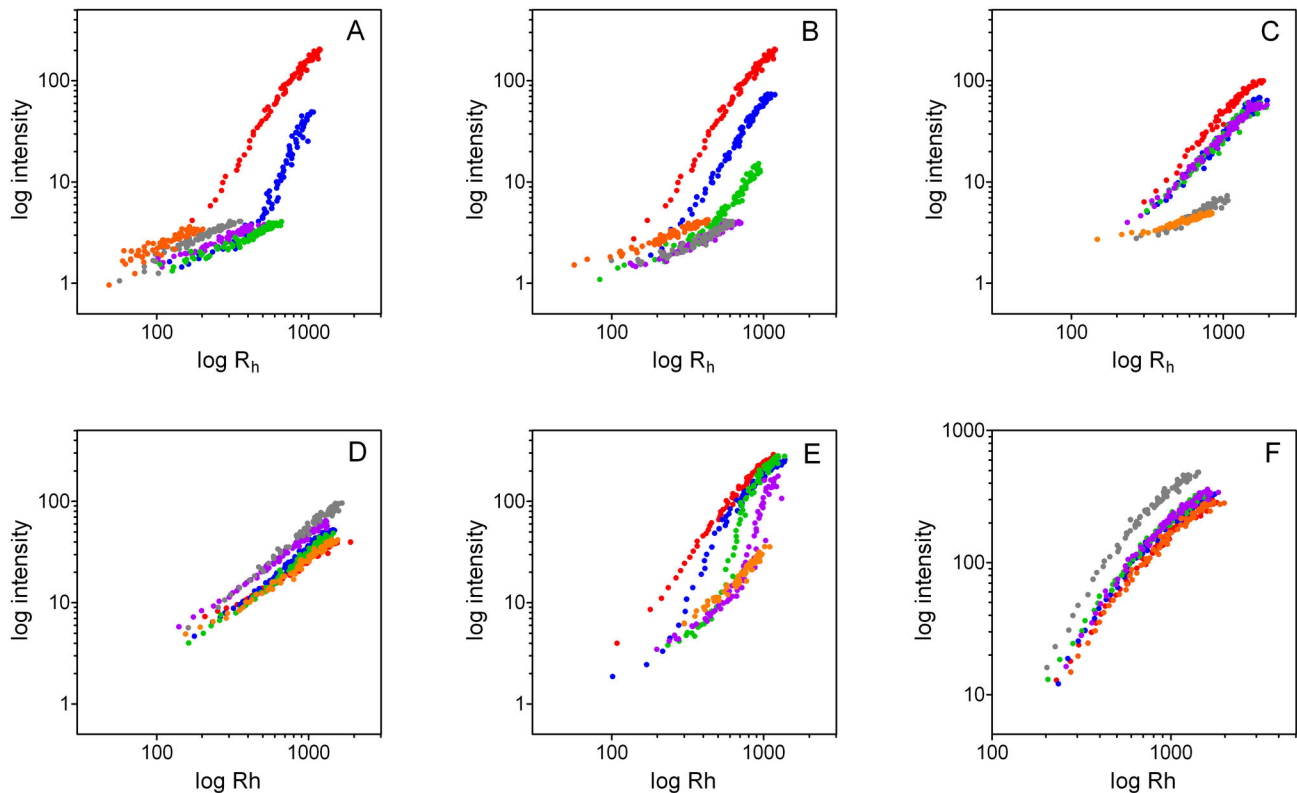
Figure 5. Dependence of dynamic-light-scattering intensity on hydrodynamic radius. Intensity data shown in Figure 2 were plotted against hydrodynamic radius data shown in Figure 4.
A. YGlapS.
B. YEpS.
C. YGlaS.
doi: 10.1371/journal.pone.0080344.g005

concentrations up to 20 µg/ml. From scanning electron micrographs, COM and COD crystals could readily be distinguished from one another: the former are penetration twins with monoclinic symmetry, the latter are rectangular bipyramids (Figure 6). Under control (no peptide) conditions,there was very little COD formation (Figure 6A). In the presence of higher concentrations of YGlapS or YEpS, COD crystals were commonly seen (Figure 6C, F). At lower concentrations of these phosphopeptides or at high concentrations of SK-Gla, COM crystals were smaller, with rounder interfacial edges, rough surfaces and apparent loss of twinning (Figure 6B, E, I).

To quantify these effects, mean crystal volumes (μm^3) and mean crystal densities (crystals/mm^2) were measured for each crystal polymorph. The mean volumes and densities were then combined to give total volumes of COM and COD ($\mu m^3/mm^2$). Data obtained at 20 µg/ml peptide are shown in Figure 7. Comparison of panels C and F shows that, in the absence of

peptide, formation of COM is greatly favored over COD under the conditions used.

COM data are shown in the upper panels of Figure 7. All peptides except YGlaS significantly decreased the mean size of COM crystals, although the phosphopeptides YGlapS and YEpS had by far the most inhibitory effects (Figure 7A). YES, which increased the number of COM crystals formed, was the only peptide to significantly affect this value (Figure 7B). Combining mean crystal sizes and densities showed that only YGlapS and YEpS significantly decreased total COM volumes (Figure 7C).

COD data are shown in the lower panels of Figure 7. None of the peptides caused a significant effect on mean COD volume (Figure 7D). Only YGlapS significantly increased the density of COD crystals (Figure 7E). Total volumes of COD were significantly increased by both YGlapS and YEpS (Figure 7F).

The effects of peptide concentration on calcium oxalate crystallization are shown in Figure 8. YGlapS exhibited almost complete inhibition of COM formation at 1 µg/ml, whereas
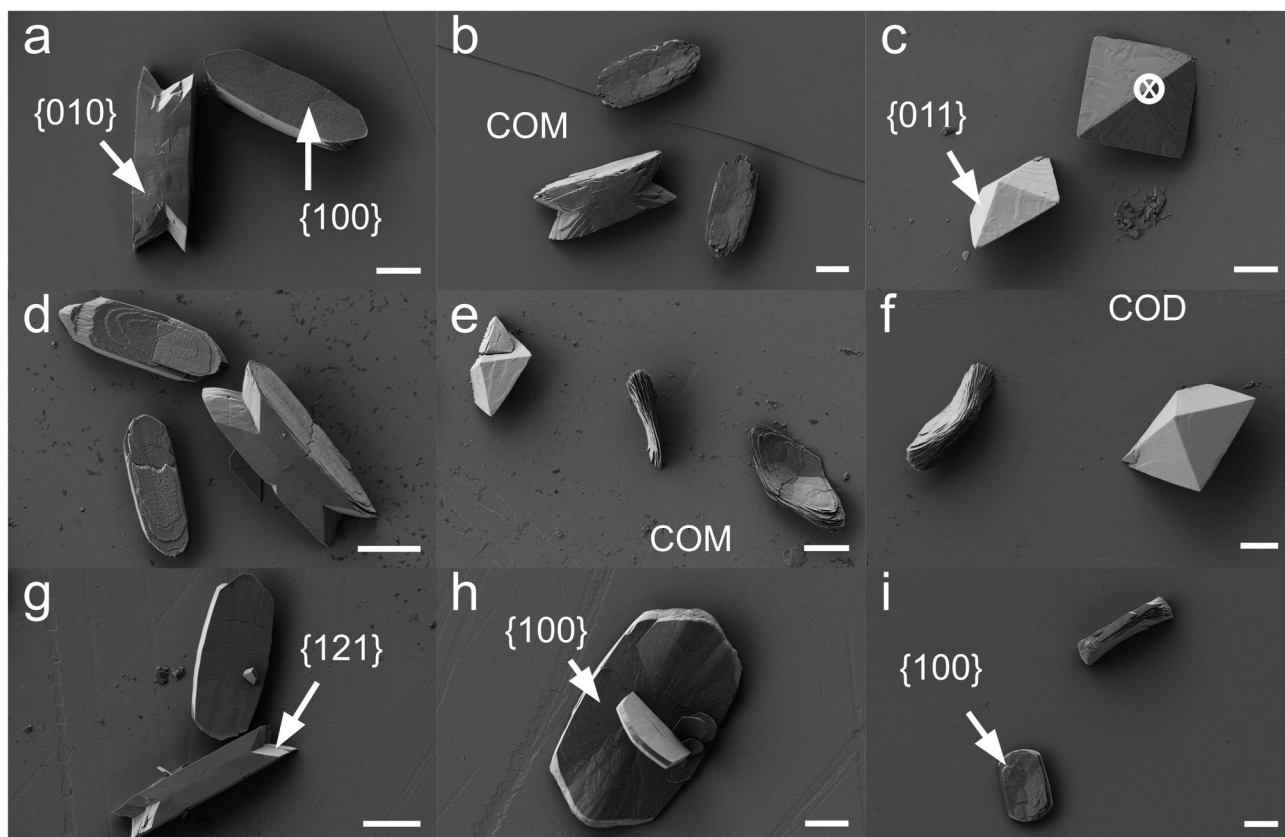
Figure 6. Scanning electron microscopy of CaOx crystals grown in the presence and absence of MGP peptides. A. Control (scale bar 4 µm).
B. YGlapS, 1 µg/ml (scale bar 6 µm) .
C. YGlapS, 5 µg/ml (cross – view parallel to <001>) (scale bar 4 µm) .
D. YEpS, 1 µg/ml (scale bar 4 µm).
E. YEpS, 5 µg/ml (scale bar 4 µm).
F. YEpS, 20 µg/ml (scale bar 4 µm).
G. SK-Gla, 5 µg/ml (scale bar 6 µm).
H. SK-Gla, 10 µg/ml (scale bar 4 µm).
I. SK-Gla, 20 µg/ml (scale bar 6 µm).
Arrows point to the three faces developed in penetration twin COM crystals (Miller indices {100}, {010} and {121}) and the single face developed in bipyramid COD crystals (Miller index {011}) [28].
doi: 10.1371/journal.pone.0080344.g006

YEpS only achieved a comparable level of inhibition at a concentration of 20 µg/ml (Figure 8A). The effect of the phosphopeptides on COD formation appears to be biphasic, with higher COD volumes seen at a YGlapS or YEpS concentration of 5 µg/ml than at 10 µg/ml (Figure 8B).

Discussion

Most mineral-binding proteins are disordered; in fact, these proteins have been claimed to be the most disordered class of proteins [31]. We recently suggested that this lack of order assists proteins in interacting with mineral crystals, by facilitating sequential formation of ionic bonds [32]. However, some mineral-binding proteins are well-folded. Osteocalcin, a gla-containing protein that is essentially restricted to mineralized tissues, has been shown to adsorb to HA and inhibit HA formation [33,34]. By NMR spectroscopy [35] and X-ray diffraction [36], it was shown that, while OC is mostly α-helical, its N-terminus is disordered. Interestingly, the 3 gla residues are all within a single helical segment and project from the same face of the helix.

CD analysis of the MGP peptides used in the present study revealed an almost complete absence of α-helix. It may be that the 14-mer peptides are too short to fold independently. An analysis of MGP using PONDR (Predictor of Naturally Disordered Proteins) suggested that the sequences corresponding to YGlapS and SK-Gla are disordered, but most of the remainder of the molecule is ordered (unpublished).
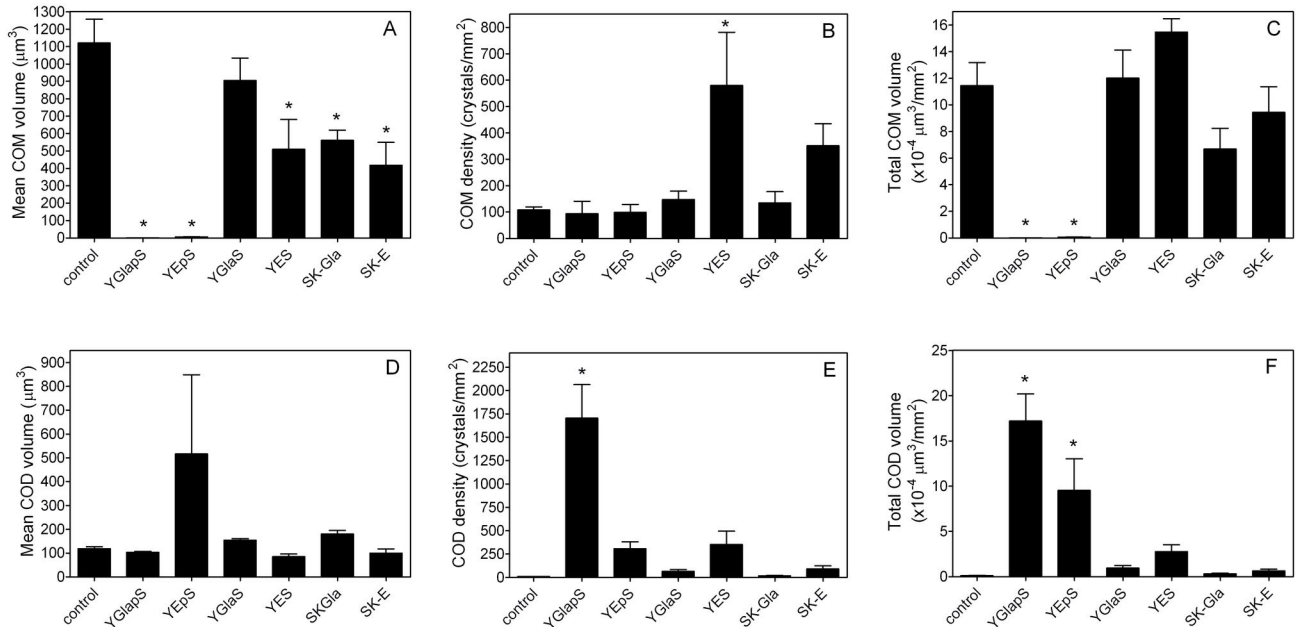
Figure 7. Effect of MGP peptides on calcium oxalate crystallization as measured by scanning electron microscopy. All peptides were used at 20 µg/ml.
A. Mean COM crystal volume.
B. COM crystal density.
C. Total COM volume (A x B).
D. Mean COD crystal volume.
E. COD crystal density.
F. Total COD volume (D x E).
Error bars represent standard error of themean. *Significantly different from control, P<0.01.
doi: 10.1371/journal.pone.0080344.g007
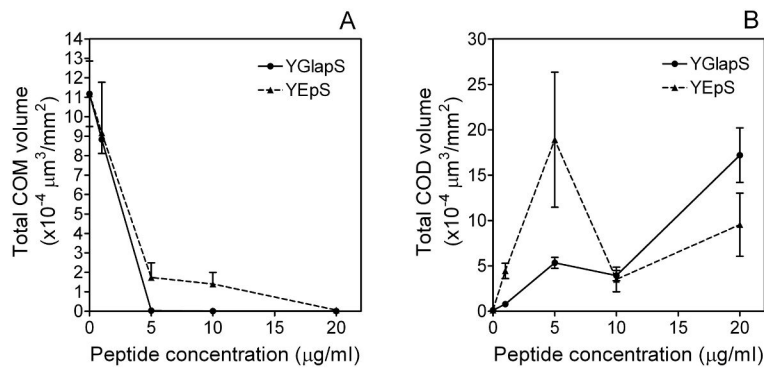
Figure 8. Effects of YGlapS and YEpS on COM (A) and COD (B) formation as measured by scanning electron microscopy. Error bars represent standard error of the mean.
doi: 10.1371/journal.pone.0080344.g008

The effects of these peptides on HA formation were studied by DLS. DLS intensities are a function of both the concentration and size of scattering particles. The average hydrodynamic radius (R_h) of the scattering particles can be calculated from the decay rate of the autocorrelation function of the scattered intensity. It is not feasible to measure the concentration of scatters directly. If the scattering particles are crystals in a supersaturated solution, a time-dependent increase in DLS intensity can be due to either nucleation (increased concentration of crystals) or growth (increased size of crystals). As the change in R_h over time is a measure of crystal growth, we were able to determine the effects of MGP

peptides on HA growth. To gain insight into the effects of MGP peptides on crystal nucleation, we plotted intensity against R_h over a range of peptide concentrations. If a peptide reduces the intensity of light scattered over a range of hydrodynamic radii, this can only due to a reduction in the concentration of scattering particles – i.e., inhibition of crystal nucleation. By these means, we were able, for the first time, to study the effects of MGP peptides on HA nucleation.

According to the above definitions of crystal formation, nucleation and growth, 4 of the 6 MGP peptides studied inhibit HA formation, in the order YGlapS > YEpS > YGlaS > SK-Gla, with YES and SK-E having no effect. The same four peptides inhibited HA growth, in the same order of potency, with YES and SK-E again having no inhibitory effect. Three of the peptides inhibited HA nucleation, in the order YGlapS > YEpS > YGlaS, with YES, SK-Gla and SK-E having no effect.

Based on these findings we conclude that, in general, MGP peptides that inhibit HA growth also inhibit nucleation of HA. The exception was SK-Gla, which had a weak effect on nucleation and none on growth.

Comparisons between post-translationally modified and non-post-translationally versions of the same peptide allow us to deduce the relative importances of phosphate and γ-carboxylate groups in the inhibition of HA formation. In terms of DLS intensity, YGlapS was more potent ($IC_{50}I$ = 0.234 μM) than YEpS ($IC_{50}I$ = 0.335 μM), which in turn was more potent than YGlaS ($IC_{50}I$ = 2.80 μM). In terms of R_h, the IC_{50} values measured for YGlapS, YEpS and YGlaS were 1.76, 3.15 and 5.44 μM, respectively. Although we were not able to quantify the effects of these peptides on HA nucleation, it is clear that the same order of potency obtains. These analyses show that, although both phosphate and γ-carboxylate groups contribute to the HA-inhibiting activity of the YGlapS peptide, which corresponds to amino acids 1-14 of human MGP, phosphate groups are more important. This is not surprising, as the peptide has 3 phosphoserines and only one gla.

In general, it appears that the role of protein anionic groups in adsorption to biomineral crystals is simply to contribute to the net negative charge of the protein [23,37]. Note that the order of potency of MGP peptides in inhibiting HA nucleation and growth corresponds exactly to order of peptide negative charge (Table 1). There is no compelling reason to believe that there is any specificity with respect to the chemical nature of the charged group, only with respect to its net charge.

A novel aspect of the present study is that the effects of MGP peptides on CaOx formation were analyzed. Only two peptides, YGlapS and YEpS, caused a significant decrease in the total volume of COM. This was entirely due to inhibition of COM growth, as the number of crystals nucleated was not affected by these peptides. As described above, YGlapS and

YEpS are also the most potent inhibitor of HA formation as measured by DLS. In that case, however, the effect is on crystal nucleation and growth.

Another difference between the effects of MGP peptides on HA and calcium oxalate crystallization is that, in the latter case, inhibition of COM formation by YGlapS or YEpS is associated with concomitant formation of COD – a CaOx polymorph that is not normally favoured under the conditions used. From our measurements of COD density and average volume, it is clear that the effect of YGlapS is entirely on nucleation, while the effect of YEpS appears to be on both nucleation and growth (although neither is significantly increased). Inhibition of COM and promotion of COD are also mediated by highly anionic peptides of the mineral-binding protein osteopontin [29,38]. In that case, and presumably in the present one, nucleation of specific COD faces by peptide adsorbed to the mica substrate appears to be responsible.

This is the first study showing that MGP inhibits calcium oxalate crystallization. We suggest that MGP, like osteopontin and Tamm-Horsfall protein, plays a role in preventing stone formation in kidney. MGP is quite highly expressed in kidney [1] but has not been reported in the urine [39,40]. Therefore, as in blood vessels, this protein is probably confined to the extracellular matrix of the nephron. We therefore speculate that MGP acts to inhibit crystal formation in the subepithelial connective tissue, whereas osteopontin and Tamm-Horsfall protein prevent crystallization in the urine.

In conclusion, we have shown that highly anionic MGP peptides, particularly the N-terminal peptide YGlapS and its non-γ-carboxylated counterpart YEpS, inhibit the formation of two biominerals implicated in ectopic calcification, HA and COM. By use of novel approaches, we have been able to distinguish between effects on crystal nucleation and crystal growth. In the case of HA, nucleation and growth are both inhibited by MGP peptides. In the case of COM, only growth is inhibited; this is associated with the concomitant formation of COD, a less-stable polymorph of CaOx.

Acknowledgements

Author Contributions

Conceived and designed the experiments: JRdB HAG GKH BG. Performed the experiments: MG JD JSG YL. Analyzed the data: MG BG GKH. Wrote the manuscript: GKH.

References

1. Fraser JD, Price PA (1988) Lung, heart, and kidney express high levels of mRNA for the vitamin K-dependent matrix Gla protein. Implications for the possible functions of matrix Gla protein and for the tissue distribution of the gamma-carboxylase. J Biol Chem 263: 11033-11036. PubMed: 3042764.

2. Price PA, Williamson MK (1985) Primary structure of bovine matrix Gla protein, a new vitamin K-dependent bone protein. J Biol Chem 260: 14971-14975. PubMed: 3877721.

3. Price PA, Rice JS, Williamson MK (1994) Conserved phosphorylation of serines in the Ser-X-Glu/Ser(P) sequences of the vitamin K-dependent matrix Gla protein from shark, lamb, rat, cow, and human. Protein Sci 3: 822-830. PubMed: 8061611.

4. Price PA, Urist MR, Otawara Y (1983) Matrix Gla protein, a new gamma-carboxyglutamic acid-containing protein which is associated with the organic matrix of bone. Biochem Biophys Res Commun 117: 765-771. doi:10.1016/0006-291X(83)91663-7. PubMed: 6607731.

5. Hackeng TM, Rosing J, Spronk HMH, Vermeer G (2001) Total chemical synthesis of human matrix Gla protein. Protein Sci 10: 864-870. doi:10.1110/ps.44701. PubMed: 11274477.

6. Luo G, Ducy P, McKee MD, Pinero GJ, Loyer E et al. (1997) Spontaneous calcification of arteries and cartilage in mice lacking matrix GLA protein. Nature 386: 78-81. doi:10.1038/386078a0. PubMed: 9052783.

7. Price PA, Faus SA, Williamson MK (1998) Warfarin causes rapid calcification of the elastic lamellae in rat arteries and heart valves. Arterioscler Thromb Vasc Biol 18: 1400-1407. doi:10.1161/01.ATV.18.9.1400. PubMed: 9743228.

8. Canfield AE, Farrington C, Dziobon MD, Boot-Handford RP, Heagerty AM et al. (2002) The involvement of matrix glycoproteins in vascular calcification and fibrosis: an immunohistochemical study. J Pathol 196: 228-234. doi:10.1002/path.1020. PubMed: 11793375.

9. Ueland T, Gullestad L, Dahl CP, Aukrust P, Aakhus S et al. (2010) Undercarboxylated matrix Gla protein is associated with indices of heart failure and mortality in symptomatic aortic stenosis. J Intern Med 268: 483-492. doi:10.1111/j.1365-2796.2010.02264.x. PubMed: 20804515.

10. Villines TC, O'Malley PG, Feuerstein IM, Thomas S, Taylor AJ (2009) Does Prolonged Warfarin Exposure Potentiate Coronary Calcification in Humans? Results of the Warfarin and Coronary Calcification Study. Calcif Tissue Int 85: 494-500. doi:10.1007/s00223-009-9300-4. PubMed: 19847375.

11. Schurgers LJ, Spronk HM, Skepper JN, Hackeng TM, Shanahan CM et al. (2007) Post-translational modifications regulate matrix Gla protein function: importance for inhibition of vascular smooth muscle cell calcification. J Thromb Haemost 5: 2503-2511. doi:10.1111/j.1538-7836.2007.02758.x. PubMed: 17848178.

12. Grohe B, O'Young J, Ionescu DA, Lajoie G, Rogers KA et al. (2007) Control of calcium oxalate crystal growth by face-specific adsorption of an osteopontin phosphopeptide. J Am Chem Soc 129: 14946-14951. doi:10.1021/ja0745613. PubMed: 17994739.

13. Tomson MB, Nancollas GH (1978) Mineralization kinetics: a constant composition approach. Science 200: 1059-1060. doi:10.1126/science.200.4345.1059. PubMed: 17740700.

14. O'Young J, Liao YY, Xiao YZ, Jalkanen J, Lajoie G et al. (2011) Matrix Gla Protein Inhibits Ectopic Calcification by a Direct Interaction with Hydroxyapatite Crystals. J Am Chem Soc 133: 18406-18412. doi:10.1021/ja207628k. PubMed: 21961692.

15. Roberto VP, Cavaco S, Viegas CSB, Simes DC, Ortiz-Delgado JB et al. (2009) Matrix Gla protein in turbot (Scophthalmus maximus): Gene expression analysis and identification of sites of protein accumulation. Aquaculture 294: 202-211. doi:10.1016/j.aquaculture.2009.06.020.

16. Gavaia PJ, Simes DC, Ortiz-Delgado JB, Viegas CSB, Pinto JP et al. (2006) Osteocalcin and matrix Gla protein in zebrafish (Danio rerio) and Senegal sole (Solea senegalensis): Comparative gene and protein expression during larval development through adulthood. Gene Expr Patterns 6: 637-652. doi:10.1016/j.modgep.2005.11.010. PubMed: 16458082.

17. Yasui T, Fujita K, Sasaki S, Sato M, Sugimoto M et al. (1999) Expression of bone matrix proteins in urolithiasis model rats. Urol Res 27: 255-261. doi:10.1007/s002400050119. PubMed: 10460895.

18. Wang L, Raikwar N, Deng L, Yang M, Liang L et al. (2000) Altered gene expression in kidneys of mice with 2,8-dihydroxyadenine nephrolithiasis. Kidney Int 58: 528-536. doi:10.1046/j.1523-1755.2000.00199.x. PubMed: 10916076.

19. Gao B, Yasui T, Itoh Y, Tozawa K, Hayashi Y et al. (2007) A polymorphism of matrix Gla protein gene is associated with kidney stones. J Urol 177: 2361-2365. doi:10.1016/j.juro.2007.01.118. PubMed: 17509359.

20. Lu XL, Gao B, Liu ZH, Tian XR, Mao X et al. (2012) A polymorphism of matrix Gla protein gene is associated with kidney stone in the Chinese Han population. Gene 511: 127-130. doi:10.1016/j.gene.2012.09.112. PubMed: 23046575.

21. Estepa L, Daudon M (1997) Contribution of Fourier transform infrared spectroscopy to the identification of urinary stones and kidney crystal deposits. Biospectroscopy 3: 347-369. doi:10.1002/(SICI)1520-6343(1997)3:5.

22. Uvarov V, Popov I, Shapur N, Abdin T, Gofrit ON et al. (2011) X-ray diffraction and SEM study of kidney stones in Israel: quantitative analysis, crystallite size determination, and statistical characterization. Environ Geochem Health 33: 613-622. doi:10.1007/s10653-011-9374-6. PubMed: 21308400.

23. Grohe B, Taller A, Vincent PL, Tieu LD, Rogers KA et al. (2009) Crystallization of Calcium Oxalates Is Controlled by Molecular Hydrophilicity and Specific Polyanion-Crystal Interactions. Langmuir 25: 11635-11646. doi:10.1021/la901145d. PubMed: 19725562.

24. Hopp TP, Woods KR (1981) Prediction of protein antigenic determinants from amino acid sequences. Proc Natl Acad Sci U S A 78: 3824-3828. doi:10.1073/pnas.78.6.3824. PubMed: 6167991.

25. de Bruyn JR, Goiko M, Mozaffari M, Bator D, Dauphinee RL et al. (2013) Dynamic light scattering study of inhibition of nucleation and growth of hydroxyapatite crystals by osteopontin. PLOS ONE 8: e56764. doi:10.1371/journal.pone.0056764. PubMed: 23457612.

26. Berne BJ, Pecora R (1976) Dynamic Light Scattering: with Applications to Chemistry, Biology, and Physics. New York: Wiley.

27. Frisken BJ (2001) Revisiting the method of cumulants for the analysis of dynamic light-scattering data. Appl Opt 40: 4087–4091. doi:10.1364/AO.40.004087. PubMed: 18360445.

28. Taller A, Grohe B, Rogers KA, Goldberg HA, Hunter GK (2007) Specific adsorption of osteopontin and synthetic polypeptides to calcium oxalate monohydrate crystals. Biophys J 93: 1768-1777. doi:10.1529/biophysj.106.101881. PubMed: 17496021.

29. Chan BP, Vincent K, Lajoie GA, Goldberg HA, Grohe B et al. (2012) On the catalysis of calcium oxalate dihydrate formation by osteopontin peptides. Colloids Surf B Biointerfaces 96: 22-28. doi:10.1016/j.colsurfb.2012.03.015. PubMed: 22503630.

30. Koenigsberger E, Koenigsberger LC (2001). Pure Appl Chem 73: 785. doi:10.1351/pac200173050785.

31. Kalmar L, Homola D, Varga G, Tompa P (2012) Structural disorder in proteins brings order to crystal growth in biomineralization. Bone 51: 528-534. doi:10.1016/j.bone.2012.05.009. PubMed: 22634174.

32. Hunter GK, O'Young J, Grohe B, Karttunen M, Goldberg HA (2010) The flexible polyelectrolyte hypothesis of protein-biomineral interaction. Langmuir 26: 18639-18646. doi:10.1021/la100401r. PubMed: 20527831.

33. Hauschka PV, Carr SA (1982) Calcium-dependent alpha-helical structure in osteocalcin. Biochemistry 21: 2538-2547. doi:10.1021/bi00539a038. PubMed: 6807342.

34. Price PA, Poser JW, Raman N (1976) Primary structure of the gamma-carboxyglutamic acid-containing protein from bovine bone. Proc Natl Acad Sci U S A 73: 3374-3375. doi:10.1073/pnas.73.10.3374. PubMed: 1068450.

35. Dowd TL, Rosen JF, Li L, Gundberg CM (2003) The three-dimensional structure of bovine calcium ion-bound osteocalcin using 1H NMR spectroscopy. Biochemistry 42: 7769-7779. doi:10.1021/bi034470s. PubMed: 12820886.

36. Hoang QQ, Sicheri F, Howard AJ, Yang DS (2003) Bone recognition mechanism of porcine osteocalcin from crystal structure. Nature 425: 977-980. doi:10.1038/nature02079. PubMed: 14586470.

37. Grohe B, O'Young J, Ionescu A, Lajoie G, Rogers KA et al. (2007) Control of calcium oxalate crystal growth by face-specific adsorption of an osteopontin phosphopeptide. J Am Chem Soc 129: 14946-14951. doi:10.1021/ja0745613. PubMed: 17994739.

38. Grohe B, Chan BP, Sørensen ES, Lajoie G, Goldberg HA et al. (2011) Cooperation of phosphates and carboxylates controls calcium oxalate crystallization in ultrafiltered urine. Urol Res 39: 327–338. doi:10.1007/s00240-010-0360-8. PubMed: 21234554.

39. Oh J, Pyo JH, Jo EH, Hwang SI, Kang SC et al. (2004) Establishment of a near-standard two-dimensional human urine proteomic map. Proteomics 4: 3485-3497. doi:10.1002/pmic.200401018. PubMed: 15529407.

40. Tyan YC, Guo HR, Liu CY, Liao PC (2006) Proteomic profiling of human urinary proteome using nano-high performance liquid chromatography/electrospray ionization tandem mass spectrometry. Anal Chim Acta 579: 158-176. doi:10.1016/j.aca.2006.07.033. PubMed: 17723740.